Hindawi Publishing Corporation
Advances in Condensed Matter Physics
Volume 2015, Article ID 475890, 14 pages
http://dx.doi.org/10.1155/2015/475890

Research Article

The Electronic Structure of Short Carbon Nanotubes: The Effects of Correlation

Vijay Gopal Chilkuri,[1] Stefano Evangelisti,[1] Thierry Leininger,[1] and Antonio Monari[2,3]

[1]*Laboratoire de Chimie et Physique Quantiques, IRSAMC, Université de Toulouse et CNRS, 118 Route de Narbonne, 31062 Toulouse Cedex, France*
[2]*Université de Lorraine, Nancy, Théorie-Modélisation-Simulation, SRSMC, Boulevard des Aiguillettes, 31062 Vandœuvre-lès-Nancy, France*
[3]*CNRS, Théorie-Modélisation-Simulation, SRSMC, Boulevard des Aiguillettes, 31062 Vandœuvre-lès-Nancy, France*

Correspondence should be addressed to Stefano Evangelisti; stefano.evangelisti@irsamc.ups-tlse.fr

Received 20 April 2015; Revised 16 July 2015; Accepted 5 August 2015

Academic Editor: Ashok Chatterjee

This paper presents a *tight binding* and *ab initio* study of finite zig-zag nanotubes of various diameters and lengths. The vertical energy spectra of such nanotubes are presented, as well as their spin multiplicities. The calculations performed using the *tight binding* approach show the existence of quasi-degenerate orbitals located around the Fermi level, thus suggesting the importance of high-quality *ab initio* methods, capable of a correct description of the nondynamical correlation. Such approaches (Complete Active Space SCF and Multireference Perturbation Theory calculations) were used in order to get accurate ground and nearest excited-state energies, along with the corresponding spin multiplicities.

1. Introduction

Besides the two lightest elements, hydrogen and helium, carbon is one of the most widespread elements in the universe and one of the best known ones. Indeed, its three-dimension allotropic forms, diamond and graphite, are well known since the antiquity. For this reason, the recent discovery of new low-dimensional allotropic forms, such as fullerenes, carbon nanotubes, and graphene, came out rather unexpected [1, 2]. In a few years, a completely new branch of science was born, whose scientific and technological impact can hardly be overestimated. Indeed, these findings had, and still have, an enormous importance in the discovery of novel and advanced materials and have been one of the key factors in the development of nanoscience. The peculiar properties of graphene (that concern both the "infinite" ideal sheet and finite nonoislands) raise new challenging theoretical problems, whose understanding and modeling will bring significant insight in our comprehension of the structure of matter. Nanotubes, which can be obtained from a graphene stripe by enrolling it along longitudinal axes, present an even larger spectrum of interesting behaviors. It is clear that a better understanding of these systems would make our knowledge of the general properties of solid-state physics and chemistry much deeper.

The new allotropic forms of carbon share the particularity of being all of low dimensionality. Indeed, the almost spherical fullerene [3] can be considered as a quasi-zero-dimensional (0D) structure, while the graphene one-atom-thick surface is a strictly two-dimensional (2D) structure. Between these two extreme cases are located the carbon nanotubes that can be considered as essentially one-dimensional (1D) materials. The presence of carbon π-conjugated lattice, usually resembling a honeycomb hexagonal lattice, is the common feature to all these forms and is at the origin of their striking properties. Indeed, the strength of the carbon-carbon sigma bond and the rigidity of the resulting structure confer graphene and nanotubes a great stability and rigidity and make them appealing to be used as building-block fibers for materials having to resist considerable stress [4]. Another remarkable aspect that should be stressed is the hydrophobicity and the resistance of these materials, a fact

that makes them ideal candidates for drug delivery and vectorization [5]. In addition to these *mechanical* properties, which are already extensively exploited nowadays, there are also peculiar and surprising *electronic* properties exhibited by these materials. For instance, graphene can be considered as a zero-gap semiconductor showing an infinite electronic mobility at the Fermi level. Carbon nanotubes [6], on the other hand, which are formally obtained by enrolling a graphene sheet along a helicoidal symmetry axis, show a vast variety of electronic behaviors. They exhibit extremely interesting properties, with a quite complex and rich structure-property correlation pattern. In particular, depending on the way the original graphene sheet is enrolled around the axis, nanotubes can present or not chirality, and their conductivity properties can vary dramatically. So different classes of nanotubes can present a behavior that passes from metallic to low-gap semiconductor, to real semiconductor materials. This peculiar characteristic can efficiently be exploited in the field of opto- and molecular-electronics devices: the potential performance and efficiency of carbon based nanostructures could potentially induce a revolution in that field, comparable to the one produced by silicon based microdevices [1, 7].

Because of the scientific and technological importance of carbon nanotubes, a huge amount of scientific work, both theoretical and experimental, has been devoted to the study of the properties and the electronic structure of these systems. Up to now, however, the great majority of such studies were conducted on infinitely extended systems. Moreover, in many cases, the Hamiltonians used were restricted to semiempirical models, *ab initio* calculations being more often performed at density functional theory level only. However, even if the study of extended systems deserves a considerable importance, both from a theoretical and a practical point of view, finite-size effects occurring in short finite clusters can also reveal new and unexpected properties, which can strongly modify the physical behavior with respect to the infinite system. In particular, it is known that graphene nanoclusters and open carbon nanotubes can present the so-called edge orbitals that are partially filled orbitals whose electron density is mainly concentrated on the border regions of the system. A peculiarity of these orbitals is given by the fact that their energy lies close to the Fermi level; that is, they are the frontier orbitals of the system. Depending on the geometry of the cluster, the edge orbitals show interesting degeneracy patterns. These features will imply the presence of different types of open-shell electronic structures, possibly inducing magnetic behaviors, characterized by a high-spin ground state. Moreover, there is the possibility of a closing of the Fermi level gap, to give rise to a metallic behavior in the limit of large systems.

The presence of an open-shell structure will also induce a strong multiconfigurational nature of the low-lying states of the system (in particular, of those of lower multiplicity). This fact implies that multireference methods are required to properly take into account the effects of the static correlation [8]. Note, as previously evoked, that the magnetic behavior is strongly dependent on the geometry of the cluster and can be rationalized by invoking the Ovchinnicov Rule [9, 10] and Lieb's theorem [11]. For instance, it has been argued that triangular-shape clusters are ferromagnetic, while hexagonal shapes are expected to be diamagnetic and show a gap at the Fermi level. Note also that the magnitude of the magnetic coupling between the states can be tuned by varying the size of the cluster. All these important characteristics can been exploited by connecting in a network different graphene clusters characterized by different magnetic properties. Let us also cite the fact that the required precise control on the shape and size of the cluster can nowadays be achieved by bottom-up techniques based on the precise deposition of carbon atoms on different surfaces. In fact, such techniques have already allowed to produce very specific graphene clusters, and even graphene antidots [12]. Finally, it is also noteworthy to remind that carbon nanostructures can be used to host and stabilize magnetic linear structures and that the interaction with conjugated carbon structures can also strongly modify the magnetic behavior of the linear aggregate.

In the present contribution, we want to extend our analysis of border effects performed on graphene nanoclusters to the domain of nanotubes. In particular we will concentrate on zig-zag nonchiral nanotubes, and we will consider only open structures that present terminal edges saturated with hydrogens. Indeed, this simple choice allows to keep all the carbon atoms sp^2-hybridized and to limit the edge effects. This is often done in theoretical studies even if in most experimental samples there are no terminal hydrogens.

Infinite nanotubes are uniquely characterized (apart from the sign of helicity, if they are chiral) by a pair of non-negative integer numbers, n and m (with $m \leq n$), and the corresponding nanotube is denoted as (n, m). These two numbers describe how a graphene sheet is enrolled around the helicoidal axes in order to generate the infinite nanotube. As the two extreme cases we find nonchiral nanotubes: the zig-zag nanotubes are of the type $(n, 0)$, while the corresponding armchair structures are of type (n, n). When m is different from both 0 and n, we have chiral nanotubes. If finite nanotubes are considered, the situation is much more complex, since one must consider not only the length of the nanotube itself, but also the details of its two borders. This is particularly true for chiral nanotubes, whose helicity prevents the possibility of cutting the extremities in such a way to respect the nanotube symmetry along the central axis. Nonchiral nanotubes, however, can be truncated in such a way that the two edges respect the nanotube symmetry. In zig-zag nanotubes (the systems that are the object of this work) the integer number n indicates the number of contiguous hexagon units that we find on a circular path around the tube; the m value, on the other hand, is redundant, since it is identically equal to 0. Finite-length zig-zag nanotubes are characterized by n, as the corresponding infinite systems, and by the *length* of the nanotube. We will indicate by p this length, and, in order to avoid confusion with the well-established notation (n, m), we indicate by (n_p) a fragment of a $(n, 0)$ (i.e., zig-zag) nanotube having length p.

To study the nature of edge orbitals and their influence on the global electronic structure of the nanostructure, as well as its evolution with the different nanotube structural parameters, we will apply two different computational strategies: a very simple semiempirical Hückel approach, which

can treat a large variety of different structures, and highly correlated multireference wave-function-based approaches, able to give quantitative results but whose use is restricted to relatively small systems. The first crude approximation allows us to obtain a qualitative overview of the density of states and in particular to characterize the orbital degeneracies at the Fermi level. Note that this approach will also allow us to consider very large aggregates, that is, to come close to the infinite system limit. The wave-function-based approach, on the other hand, takes care of the static and dynamic correlation and is able to study the low-lying spectrum of the magnetic states, evaluating its evolution with the geometry and the structural parameters. To the best of our knowledge, this is the first contribution applying high level Multireference Perturbation Theory (MRPT) to the study of this kind of systems. A similar approach was already applied to closed polyacenes structures [13] whereas most of previous works on nanotubes [14–22] or nanoribbons [23] principally rely on density functional theory or tight binding results. The main conclusion of studies on There also have been some studies in the solid-state community on the energy spectrum [24] and properties of single walled nanotubes [25] using sophisticated analytic tools. Similar structures as those considered consist in an antiferromagnetic coupling of two electrons localized in the edge orbitals.

This paper is organized as follows. In Section 2, Theoretical Methods, we briefly describe the methods that we employed in this study, and we justify their use. The computational details of the calculations are given in Section 3, in order to permit the reproduction of our calculations in future further studies. In Section 4, we present the nanotube structure and symmetry, along with the particular terminology used in this work. Results at the Hückel and *ab initio* level are presented and discussed in Section 5. Final conclusions are drawn in Section 6, together with plans for future works.

2. Theoretical Methods

In this section, we briefly describe the theoretical methods and the computational approaches used in the present work. The computational details concerning both the *ab initio* and the *tight binding* approaches will be discussed in detail in the next section, in order to facilitate the reproduction of our results.

Carbon nanotubes, as it is the case of most graphene-derived nanostructures, show the presence of edge molecular orbitals (MO) that are neither doubly occupied nor totally empty in the electronic ground state (see, e.g., [12]). The simplest Hamiltonian that is able to give a qualitative description of the electronic wavefunction of sp^2-hybridized carbon structures is the Hückel Hamiltonian. It is a tight binding Hamiltonian that was developed in order to describe small polyenes and in general aromatic compounds. At Hückel level, only one p atomic orbital per carbon atom is considered (the orbital that is locally orthogonal to the σ orbitals), and this defines the π system. Correspondingly, only one electron per atom is considered. Despite its simplicity, the Hückel Hamiltonian is capable of grasping the essence of the electronic structure of these systems, and their low-lying energy spectrum obtained at this level is remarkably correct. It is worth noticing that the pioneering 1947 paper on graphite (and graphene) written by Wallace describes results obtained with this type of approach [26].

As a general strategy that we employed in previous studies on other sp^2 carbon nanostructures [13, 27], we performed preliminary tight binding calculations by using the model Hückel Hamiltonian [28], in order to obtain a first approximation of the energy spectrum at one-electron level. This is very important for subsequent calculations at many-electron level by using an *ab initio* Hamiltonian, in order to clearly identify the orbitals that form a quasi-degenerate partly occupied manifold. A proper *ab initio* treatment of this group of quasi-degenerate orbitals requires the introduction of the *nondynamical correlation* [29], and this is most conveniently done by the use of the Complete Active Space Self-Consistent Field (CAS-SCF) formalism [30]. In this approach, the correlation of the electrons distributed among the quasi-degenerate orbitals (the *active* orbitals) is fully considered at a configuration interaction level. At the same time, the shape of *all* the molecular orbitals (active or not) is fully optimized self-consistently. It is known that a CAS-SCF approach is suited for a qualitative description of the low-lying energy spectrum of open-shell systems (magnetic structures, mixed-valence systems). For quantitative results, the introduction of the *dynamical correlation* is also required, since the weights of the Slater determinants belonging to the quasi-degenerate manifold can be strongly modified by the interaction. Among the possible multireference approaches, the Quasi-Degenerate Perturbation Theory is the only one that is capable of treating these relatively large systems. In particular, contracted methods have the advantage of a weak computational dependence on the dimension of the active space and can therefore be used in the present case. In this work, we chose the n-Electron Valence Perturbation Theory at second-order level (NEVPT2), because of its capability of dealing with the intruder-state problem without the need of introduction of arbitrary parameters [31, 32].

In doing a CAS-SCF calculation, the choice of the guess starting orbitals plays a key role in the final result. Indeed, being a nonlinear optimization algorithm, CAS-SCF admits a huge number of different solutions, sometimes not presenting a particular physical interest. It is also frequent, because of this nonlinear character of the formalism, to have instabilities that lead to symmetry-breaking phenomena in the case of strictly degenerate states, as the ones that characterize nanotubes having non-Abelian symmetries. In the present work, we performed High-Spin Restricted Open-Shell Hartree-Fock (ROHF) calculations on the different systems, by choosing as single-occupied orbitals precisely the orbitals that show a quasi-degenerate character at Hückel level. Once the manifold of quasi-degenerate orbitals has been identified, we performed frozen-orbital CAS-SCF (i.e., CAS-CI) calculations on this active space. It is known that, for states having nonionic character, the resulting energy spectrum is very close to the CAS-SCF one, at a considerably lower computational cost.

3. Computational Details

In the next subsections, we describe separately the *tight binding* and *ab initio* approaches.

3.1. Tight Binding. All computations at tight binding level (Hückel calculations in the language of chemists) have been performed by using a specific home-made code[33–35]. The Hückel Hamiltonian has been constructed starting from the connectivity of each carbon atom, by defining, as usual,

$$\begin{aligned} \left\langle i \left| \widehat{H} \right| i \right\rangle &= \alpha = 0, \\ \left\langle i \left| \widehat{H} \right| j \right\rangle &= \beta \gamma_{ij}, \end{aligned} \tag{1}$$

where γ_{ij} is 1 if sites i and j are connected in the nanostructure skeleton and 0 otherwise. The value of the hopping integral β should depend, in principle, on the distance between the two connected atoms i and j. However, since the C-C bonds have very similar length in all of our structures, we assumed the same values of β for all the topologically connected pair of atoms. In our calculations, this parameter was fixed to the arbitrary value $\beta = -1$. We remind that $-\beta$ is sometimes called the hopping integral in the physics literature, where it is usually indicated as t. In the section Results and Discussion, we report the energy spectrum of several nanotubes, computed at the Hückel level. This is done as a function of the orbital number. In order to facilitate the comparison between systems having a different number of orbitals, the orbital numbers are normalized in the segment $[0, 1]$.

3.2. Ab Initio. All the systems have been studied using the minimal STO-3G Gaussian basis [36] for both carbon and hydrogen. Although this basis set is certainly too small to give quantitatively reliable results, it is known to reproduce correctly the qualitative behavior of many organic and inorganic systems. Its reduced size, on the other hand, permits to investigate at a correlated *ab initio* level systems whose size is relatively large. However, in order to explore the effect of a more realistic basis set, a limited number of structures representative of each class of nanotubes have been studied with a larger basis set, the cc-pVDZ correlation consistent basis set of Dunning [37]. These are the structures characterized by $n = 6, 7$ and $p = 4, 5$ for which a $(3s2p1d)$ contraction for C and $(2s1p)$ for H were used. This corresponds to a valence double-zeta plus polarization (vdzp) basis set.

The systems' geometries have been optimized at Restricted Open-Shell Hartree-Fock (ROHF) level for the lowest-energy state. This means the triplet state for the nanotubes characterized by an even value of $n(e\_p)$ and the quintet state for the nanotubes characterized by an odd value of $n(o\_p)$.

During geometry optimization, the D_{nd} or D_{nh} symmetries have been imposed depending on the nanotubes classes. Thus, all the coordinates have been relaxed allowing the nanotube to lose its cylindrical shape. The only remaining constraint was the order of the rotation axis. Actually, due to restrictions of the Molpro quantum chemistry package [38], optimization has been carried out using the appropriate Abelian subgroups. Even if this may result in symmetry breaking of the electronic wavefunction, it never appeared for the systems considered in this work. For all the nanotubes, it appears that only slight distortions from the regular ideal cylindrical shape have been obtained. Even the terminal hydrogens just slightly point towards the axis of the nanotube. All the detailed geometries are given in the Supplementary Material available online at http://dx.doi.org/10.1155/2015/475890. At these optimized geometries, the lowest states have been studied at Complete Active Space Self-Consistent Field (CAS-SCF) level [39]. Then the effect of dynamical correlation was introduced at Multireference Perturbation Theory (MR-PT) level, using the *partially contracted* version of second-order n-Electrons Valence Perturbation Theory (NEVPT2) formalism [40–42]. In all the CAS-SCF calculations, the active space has been selected by choosing the orbitals that are strictly degenerated or quasi-degenerated, with the Hückel Hamiltonian, at the Fermi level. This means that our active spaces are either CAS(2,2) (for the (e_p) tubes) or CAS(4,4) (for the (o_p) tubes). The geometries have been optimized at ROHF level for the high-spin wavefunction. The orbitals obtained thereof have then been kept frozen for the CAS-SCF calculations on the other spin multiplicities. In this way, our calculations are actually of CAS-CI [43, 44] type which in our case give energies close to CAS-SCF ones. The NEVPT2 formalism has then been applied to these CAS-CI wavefunctions in order to recover the dynamical correlation.

Obviously, our geometrical constraints prevent Jahn-Teller distortion which could be expected in the case of degenerate orbitals. In this preliminary work, we decided not to consider this possibility. However, due to the stiffness of the nanotube backbone we believe these distortions to be of small size.

4. Electronic Structure of Carbon sp^2 Nanostructures

The net of carbon atoms forming a graphene layer is the conceptual starting point to produce most of the carbon sp^2-hybridized nanostructures. A crucial feature to rationalize the relation between structure and electronic properties, and, more generally, to study finite-size effects in these structures, is to recognize that the honeycomb graphene skeleton forms a *bipartite lattice* [12], with two compenetrating triangular sublattices A and B. Each carbon atom belonging to a graphene nanostructure is associated with one of these two sublattices, and one can speak of A-type and B-type graphene atoms, or centers. A lattice is bipartite if each A-type atom has only B-type nearest neighbors, and vice versa. So, for instance, zig-zag edges are composed of atoms that all belong to the same sublattices. A necessary condition for a lattice to be bipartite is the absence of odd-number carbon cycles. In order to rationalize the emergence of magnetic properties in graphene nanosystems, one can recall Lieb's theorem [11]. This theorem, also known as the theorem of itinerant magnetism and usually applied within the framework of the

Hubbard one-orbital model, is able to predict the total spin of the ground state in bipartite lattices. In particular, one can see that an imbalance on the number of atom in one sublattice results in a magnetic ground state with spin

$$S = \frac{|N_A - N_B|}{2}, \quad (2)$$

where N_A and N_B are the numbers of atoms of A- and B-type, respectively. It is also possible to show that, for a Hückel Hamiltonian, $|N_A - N_B|$ is also the number of eigenvalues equal to zero. It is important to note that the magnetization originates from localized edge-states that give also rise to a high density of states at the Fermi level which in turn can determine a spin polarization instability. Moreover the relation between the unbalanced number of atoms and the ground state spin implies that two centers will be ferromagnetically coupled if they belong to the same sublattice and antiferromagnetically coupled if they do not [45].

We consider now the symmetry of the (n_p) nanotubes. It is easy to see that these structures fall into two classes, according to the parity of the length p. The (n_p) tubes have D_{nh} symmetry if p is odd ((n_o) tubes) and D_{nd} symmetry for p even ((n_e) tubes). In all these cases (with the partial exception of the case $n = 2$, which is however too narrow to form a tube) we are in the presence of non-Abelian symmetry groups. We recall that our *ab initio* calculations have been performed by using Abelian subgroups of the full point group of the system. According to the parity, even (e) or odd (o) of n and p, we have the following Abelian subgroups C_{2v} for (e_e), D_{2h} for (e_o), C_{2h} for (o_e), and C_{2v} for (o_o).

We call *edge carbon atoms* the carbon atoms that are saturated with hydrogens. The role of these edge atoms is crucial in order to understand the finite-size effects in carbon nanotubes. The edge carbon atoms of the tubes of type (e_p) can support molecular orbitals (MO) of π-nature, having alternating sign on any pair of consecutive hexagons. Let us consider the MO combinations that are localized on one of the tube extremities only. At Hückel level, it is straightforward to verify that both these alternating edge combinations are eigenfunctions of the one-electron Hamiltonian corresponding to eigenvalues equal to zero. Therefore, the Hückel energy spectrum presents a pair of degenerate orbitals at the Fermi level for all (e_p) tubes, regardless of the parity of p. The situation is different as far as the *ab initio* Hamiltonian is considered, since these two localized edge combinations are no longer exact molecular orbitals of the Fock Hamiltonian. As a result, at *ab initio* level the exact degeneracy can be lost. In particular, it turns out that while the two edge orbitals are exactly degenerate for (e_e) tubes, the degeneracy is only approximated in the case of the (e_o) structures. This point can be easily understood by symmetry considerations. In fact the two localized edge orbitals are interchanged by some of the symmetry operations of the point group of the system (D_{nh} for (e_o) and D_{nd} for (e_e) tubes). For this reason, they give rise to a representation of the molecule symmetry group. In the case of (e_e) tubes, the representation is irreducible, and it still corresponds to two *exactly degenerate* molecular orbitals of the system (e.g., see Figure 6, where the two degenerate orbitals have e_3 symmetry). In the case of the (e_o) tubes, on the other hand, the two combinations belong to two different irreducible representations of the Abelian symmetry group of the system. The two orbitals are only approximately degenerate (see Figure 7, where the two orbitals have b_{1u} and b_{2g} symmetries, resp.). This argument explains the remarkable difference between the *tight binding* and *ab initio* energy spectra in the Fermi level region for the (e_o) tubes.

5. Results and Discussion

5.1. Tight Binding. Even if the tight binding approach represents a crude approximation of a chemical system, it can be extremely useful in order to sketch out some general tendencies and to elucidate the behavior of the different classes of compounds. This is particularly true in the present case, since a tight binding approach allows the treatment of very large systems due to its extremely reduced computational costs. It is possible, in this way, to explore the behavior of virtually "infinite" systems.

Short zig-zag nanotubes can be divided into four different classes, characterized by different symmetries and molecular-orbital patterns depending on the *parity* of n and p. The Hückel calculations for these classes permitted to characterize the different active spaces which were essentially confirmed at the *ab initio* level.

Nanotubes of the type (n_e) have D_{nd} symmetry, while those of type (n_o) have D_{nh} symmetry. At the Hückel level, both (e_e) and (e_o) have two exactly degenerate orbitals at the Fermi level, hosting two electrons. This is illustrated in Figures 1 and 2, where the energy spectra of (6_4) and (6_5) structures are reported. For the sake of comparison, the spectra of long, (6_100), or very wide, (100_4) and (100_5), structures are also reported in the figures. None of these spectra shows the presence of an energy gap at the Fermi level, and the wide structures have even an *infinite* density of levels at the Fermi level. Nanotubes of the types (o_e) and (o_o), on the other hand, have four quasi-degenerate levels (two quasi-degenerate pairs of exactly degenerate levels) near the Fermi level, hosting a total of four electrons. This fact is illustrated, for the (7_4) and (7_5) structures, in Figures 3 and 4. From these figures it appears that, in the case of very long (o_p) nanotubes, four degenerate isolated orbitals, hosting a total of four electrons, are located at the Fermi level. As a systematic study of large systems at the Hückel level involves a digression from the present topic, a general analysis of the four classes of the nanotubes will follow.

5.1.1. Nanotubes of Type e_e. The Hückel calculation for the nanotubes characterized by an even parity for both n and p showed that there were two orbitals at the Fermi level. The calculations, Figure 1, are shown for very wide and very long nanotubes for the purpose of comparison. The abscissa (k) represents the Hückel orbital number, mapped onto the interval $[0, 1]$. It can be seen that there is no gap at the Fermi level; this allows us to characterize such nanotubes as being

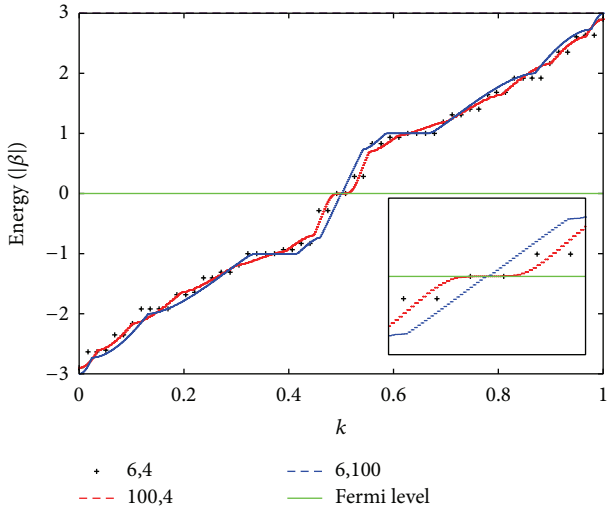

Figure 1: Hückel orbital energies for the nanotube (6_4), where $|\beta|$ is the energy unit and k is the normalized orbital number.

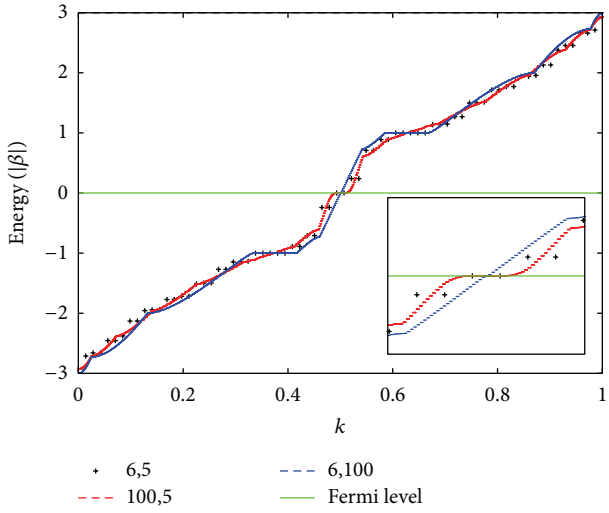

Figure 2: Hückel orbital energies for the nanotube (6_5), where $|\beta|$ is the energy unit and k is the normalized orbital number.

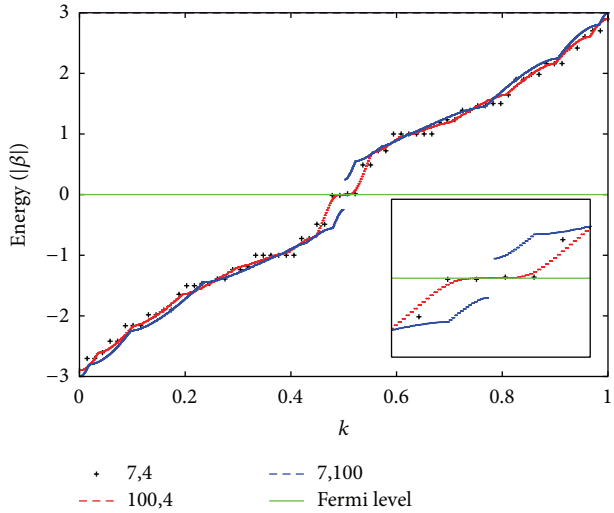

Figure 3: Hückel orbital energies for the nanotube (7_4), where $|\beta|$ is the energy unit and k is the normalized orbital number.

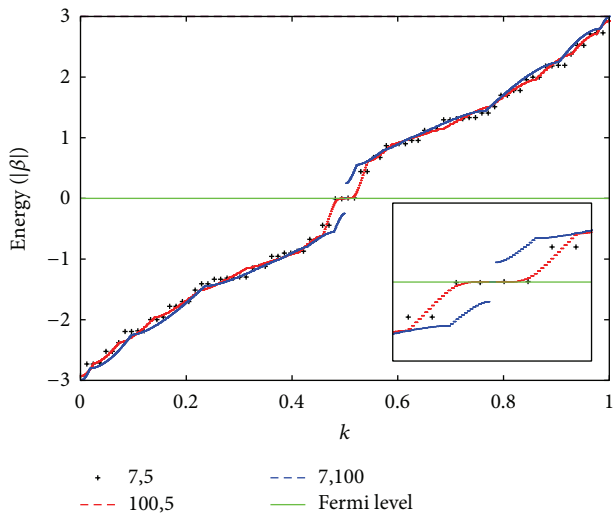

Figure 4: Hückel orbital energies for the nanotube (7_5), where $|\beta|$ is the energy unit and k is the normalized orbital number.

metallic. One can also see in Figure 1 the presence of four degenerate levels at the $|\beta| = 1$ level corresponding to the respective value of p (four in this case.)

5.1.2. Nanotubes of Type e_o. The Hückel calculations are presented in Figure 2, as one can see there are two degenerate levels similar to the previous case. It is interesting to note also that as in the previous case there is no gap at the Fermi level and one can thus characterize the nanotubes as being metallic. The figure also shows the presence of five degenerate orbitals at the level $|\beta| = 1$ as a consequence of the value of p being five.

5.1.3. Nanotubes of Type o_e. The case where the nanotubes have an odd number of rings is characteristically different from the above two cases. In the Hückel calculations shown in Figure 3, one can see the presence of four quasi-degenerate orbitals at the Fermi level. On close analysis one can distinguish pairs or orbitals which are degenerate and there is a slight energy difference between the two pairs making them quasi-degenerate. The calculations for very long nanotubes and very wide nanotubes in Figure 3 show that, in contrast to the previous two cases, where the number of hexagons (n) was a multiple of three, there is a significant gap at the Fermi level between the occupied and the virtual orbitals, making the nanotubes insulating. It is known that the infinite nanotubes characterized by n and p where n is a multiple of three are metallic, without the presence of a gap at the Fermi level (a band gap).

5.1.4. Nanotubes of Type o_o. Figure 4 represents the case characterized by an odd value of n and m. The similarity to

Table 1: The various ground state energy levels and their occupation numbers (STO-3G basis set) for the four different classes of nanotubes along with their true symmetries. It is interesting to note the abelian groups of each class: class I (6_4) = C_{2v}; class II (6_5) = D_{2h}; class III (7_4) = C_{2h}; class IV (7_5) = C_{2v}.

Nanotube	Symmetry group of the nanotube	Orbitals symmetry	High-spin ROHF orbital energy ϵ_i in au	Electronic ground state HF	Electronic ground state CAS-CI	CAS-CI occupation number n_i
6_4	D_{6d}	(i) e_3 (ii) e_3	−0.1180	$^3A_2$	$^3A_2$	1.0000
6_5	D_{6h}	(i) b_{1u} (ii) b_{2g}	−0.1176 −0.1178	$^3A_{2u}$	$^1A_{1g}$	0.9985 1.0015
7_4	D_{7d}	(i) e_{3g} (ii) e_{3g} (iii) e_{3u} (iv) e_{3u}	−0.1359 −0.1431	$^5A_{1g}$	$^1A_{1g}$	0.9517 1.0483
7_5		(i) e_1' (ii) e_1' (iii) e_1'' (iv) e_1''	−0.1384 −0.1417	$^5A_1'$	$^1A_1'$	0.9684 1.0316

the previous case is shown by the presence of two pairs of quasi-degenerate orbitals at the Fermi level and the presence of a gap between the occupied and the virtual orbitals. One can see here the presence of a number of degenerate orbitals at the $|\beta| = 1$ level.

5.2. Ab Initio. From the Hückel results, it is clear that a closed-shell determinant is never a good zero-order description of the electronic ground state of short zig-zag nanotubes. Therefore, as discussed in Computational Details, we performed ROHF calculations to optimize the geometry for the spin multiplicity that gives the minimum energy for each system. In the range of the studied values of n and p, this means triplets for the (e_p) nanotubes and quintets for the (o_p) ones. The orbitals that are obtained from these ROHF calculations are then used for the subsequent CAS-CI [39] and NEVPT2 [40–42] calculations.

We will discuss the behavior of the four classes of nanotubes of zig-zag type. As a general remark, we notice that the frontier orbitals of all four classes are localized at the edges of the tubes. This is exactly what happens at the Hückel level.

The most remarkable difference between Hückel and *ab initio* results concerns the nanotube of the type (e_o), having D_{nh} symmetry. In fact, the u and g combinations of border orbitals are obviously not degenerated at *ab initio* level, since they belong to different irreducible representations of the system point group.

However, at Hückel level, it is straightforward to check that an alternating orbital located on a single edge of the nanotube (see schematic drawings of Figure 5) is an eigenfunction of the Hamiltonian corresponding to a zero value of the energy. This implies that any combination of the two top and bottom border orbitals will be an eigenfunction with vanishing energy, so the g and u combinations are strictly degenerate. Moreover, they are completely localized on the nanotube edges.

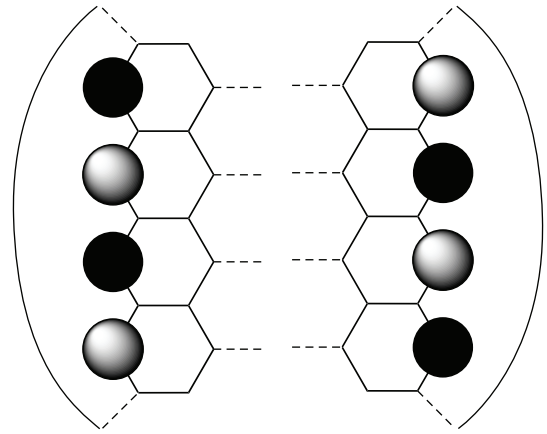

Figure 5: Scheme of the two opposite alternant Hückel edge orbitals.

5.2.1. Nanotubes of Type e_e. The nanotubes of this type have a symmetry D_{nd} where n is the number of hexagons in a ring. The highest Abelian subgroups are C_{2v} as a result of the absence of the σ_h plane contrary to the case where p is odd; see Figure 6. These nanotubes, for which the active space consisted of two orbitals, have two exactly degenerate orbitals of symmetry e_3 at the Fermi level (see Table 1) strongly localized on each edge. The geometry was optimized for the triplet state followed by CAS-CI calculations for the triplet of symmetry $^3A_2$ and the two singlets $^1A_1$ and $^1E_2$ (see Table 2).

It appears that at CAS-CI level the energy difference between the triplet and the singlet states is almost zero (of the order of 10^{-5} kJ mol^{-1} for the studied systems). This almost perfect degeneracy is removed when the effect of the dynamical correlation is introduced at NEVPT2 level. However, the ground state remains a singlet electronic state resulting from an antiferromagnetic coupling of the two

Table 2: CAS-CI and the NEVPT2 energies in kJ mol^{-1} for the class of nanotubes n_p, with n even and p even. All possible states for a CAS of two electrons in two orbitals have been calculated.

$n\backslash p$	State	2		4		6		8	
		CAS-CI	NEVPT2	CAS-CI	NEVPT2	CAS-CI	NEVPT2	CAS-CI	NEVPT2
6	$^1A_1$	$5 \cdot 10^{-4}$	−19.5	$3 \cdot 10^{-5}$	−5.9	$6 \cdot 10^{-7}$	−2.4	$3 \cdot 10^{-8}$	−1.1
	$^3A_2$	0.0	0.0	0.0	0.0	0.0	0.0	0.0	0.0
	$^1E_2$	419.8	150.8	511.9	159.2	553.2	179.9	579.0	251.7
8	$^1A_1$	$3 \cdot 10^{-3}$	−34.7	$1 \cdot 10^{-4}$	−22.3	$8 \cdot 10^{-6}$	−20.9	$1 \cdot 10^{-6}$	−24.3
	$^3A_2$	0.0	0.0	0.0	0.0	0.0	0.0	0.0	0.0
	$^1E_2$	316.3	110.8	395.5	74.9	439.6	−115.0	456.9	−553.8
10	$^1A_1$	$7 \cdot 10^{-3}$	−56.9	$4 \cdot 10^{-4}$	−63.5	$4 \cdot 10^{-5}$	−98.1	—	—
	$^3A_2$	0.0	0.0	0.0	0.0	0.0	0.0	—	—
	$^1E_2$	251.7	84.9	319.9	−60.1	354.7	−390.8	—	—

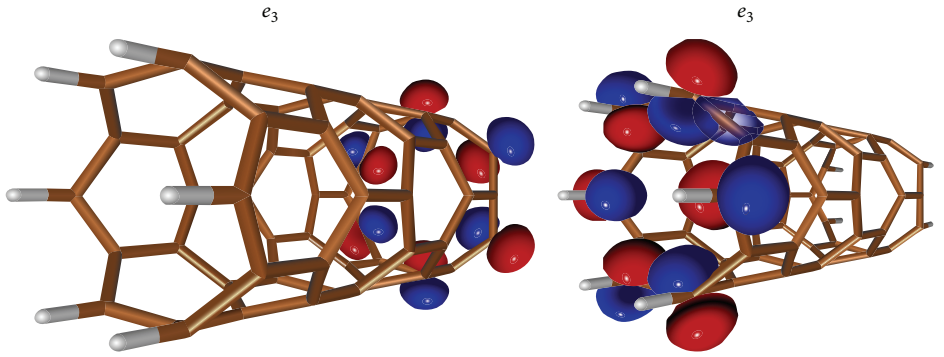

Figure 6: Active orbitals of nanotube (6_4) as an example of nanotubes with both n and p even. The orbitals are of identical size; the apparent difference in size is due to the perspective.

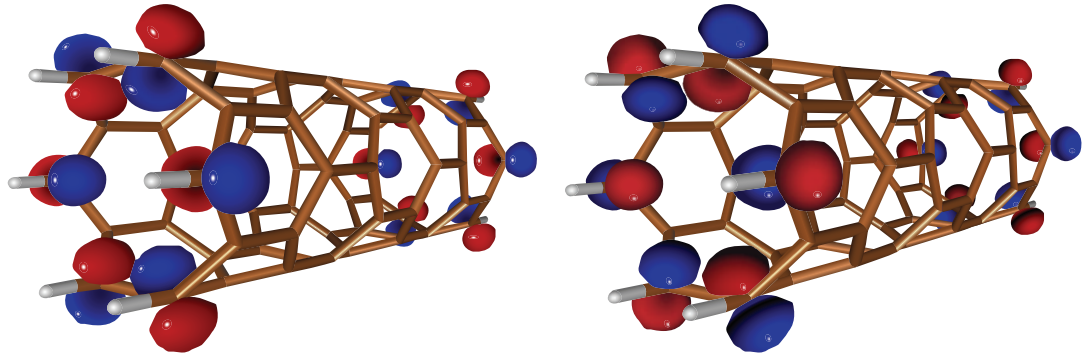

(a) b_{1u} (b) b_{2g}

Figure 7: Active orbitals of nanotube 6_5 as an example of nanotubes with n even and p odd.

electrons localized on each edge of the nanotube, whatever the length of the nanotube is.

This extremely small singlet-triplet gap at the CAS-CI increases when the effect of dynamic correlation is introduced by the NEVPT2 approach. It can also be noted that, for the case where n is six, the singlet-triplet gap decreases as the length of the nanotube is increased, going from about 20 to 1 kJ mol^{-1} as shown in Table 2. The rest of the cases show a trend where the $^1A_1$ singlet seems to be replaced by the $^1E_2$ singlet as the length is increased. Actually, state-specific CASSCF calculations virtually do not change the singlet-triplet gap as can be seen in the corresponding tables of the Supplementary Material. This remains true for all the classes of nanotubes. However, the difference between the triplet and the ionic state $^1E_2$ (see wavefunction composition in the Supplementary Material) is significantly lowered by about 261 kJ·mol^{-1}. This shows a strong modification of the orbitals which can not be overcome by the NEVPT2

Table 3: CAS-CI and the NEVPT2 energies in kJ mol^{-1} for the class of nanotubes n_p, with n even and p odd. All possible states for a CAS of two electrons in two orbitals have been calculated.

$n\backslash p$	State	1		3		5		7	
		CAS-CI	NEVPT2	CAS-CI	NEVPT2	CAS-CI	NEVPT2	CAS-CI	NEVPT2
6	$^1A_{1g}$	−0.3	−43.0	$-1 \cdot 10^{-2}$	−10.1	$-3 \cdot 10^{-4}$	−3.7	$-2 \cdot 10^{-5}$	−1.6
	$^3A_{2u}$	0.0	0.0	0.0	0.0	0.0	0.0	0.0	0.0
	$^1E_{1g}$	319.3	162.4	476.4	151.9	553.9	169.3	566.1	190.1
8	$^1A_{1g}$	−3.7	−43.1	−0.1	−25.9	$-7 \cdot 10^{-3}$	−20.7	$-9 \cdot 10^{-4}$	−21.9
	$^3A_{2u}$	0.0	0.0	0.0	0.0	0.0	0.0	0.0	0.0
	$^1E_{1g}$	237.5	138.9	364.1	79.3	417.5	−3.7	445.8	−127.1
10	$^1A_{1g}$	−12.9	−34.7	−0.6	−55.5	−0.1	−76.9	—	—
	$^3A_{2u}$	0.0	0.0	0.0	0.0	0.0	0.0	—	—
	$^1E_{1g}$	188.2	125.1	292.3	27.1	339.8	−200.4	—	—

approach. Furthermore, it has been shown that, for ionic states, NEVPT2 method is inadequate if plain CASSCF orbitals are used [46, 47]. Thus, NEVPT2 excitation energies to ionic states for the other classes are documented in the tables below but will not be discussed.

The occupation numbers of Table 1 and the CI vectors given in the Supplementary Material clearly show the multideterminantal character of the wavefunction. Indeed, for each of the states considered here, the active electrons are evenly distributed among the two active orbitals. It can also be seen that the effect of the basis set size on the wavefunction nature is completely negligible in that case.

5.2.2. Nanotubes of Type e_o. The orbitals for this case are presented in Figure 7. The nanotube has the symmetry D_{nh} as a result of the presence of a σ_h plane. The two orbitals are not localized at one edge or the other but are equally present at the two edges at the same time with gerade and ungerade symmetry, as a consequence the two orbitals are quasi-degenerate. The two orbitals are of b_{1u} and b_{2g} symmetry; see Table 1; the gerade is more stable due to the antibonding interactions between the two edge orbitals located at the ends of the nanotube.

In this case also the HF calculations and the geometry optimization were done for the triplet state and the resulting strongly localized orbitals were used for the CAS-CI/NEVPT2 calculations. These calculations were carried out for the triplet state of symmetry $^3A_{2u}$ followed by the two singlet states $^1A_{1g}$ and $^1E_{1g}$ as shown in Table 3. One can see that only the short nanotubes have $^1A_{1g}$ as the ground state at both CAS-CI and NEVPT2 level. Again, this probably arises from a strong revision of the orbitals for the higher states which is not taken into account here. At the CAS-CI level, the lowest singlet-triplet gap is very small (except for the (10_1) case which corresponds to a ring rather than a tube) and decreases with the length of the nanotube as was observed for the e_e case. At the NEVPT2 results, the trend is opposite and is even enhanced for the widest nanotubes. As in the previous case, $^1A_{1g}$ remains the ground state independently of the length at CAS-CI level. This is also true at NEVPT2 level for the smallest nanotubes, while for the larger one we observe the same limitation as for the e_e tubes.

As for the previous class of nanotubes, the wavefunction of the ground states shows a strong multideterminantal character with a equal mixing of the two configurations $|b_{1u}\overline{b_{1u}}\rangle$ and $|b_{2g}\overline{b_{2g}}\rangle$ due to the quasi-degeneracy of the two orbitals and leading to an antiferromagnetic coupling of the two electrons in the edge orbitals.

5.2.3. Nanotubes of Type o_e. The orbitals are shown in Figure 8. According to the predictions of the Hückel calculations we find four quasi-degenerate edge orbitals. The nanotube has D_{nd} symmetry with the largest Abelian subgroup being C_{2h}. The orbitals located at the edges form two pairs of degenerate orbitals; see Table 1, and on taking linear combinations of the degenerate orbitals one can construct orbitals similar to those of the type e_e, that is, two orbitals localized at one of the edges. The pairs of orbitals are separated by an energy gap due to the anti-interaction between the two edge orbitals with the ungerade orbitals being more stable than the gerade.

As for the other classes, the geometry was optimized for the high-spin quintet state at the ROHF level. The orbitals of the ROHF calculation were used in the CAS-CI/NEVPT2 calculations. These calculations were done for the quintet state and the lowest lying singlet and triplet states in each of the four symmetries of the corresponding largest Abelian group. The results are shown in Table 4. The singlet open shell of symmetry $^1A_{1g}$ is the ground state for the short nanotubes and is overtaken by the $^1A_{1u}$ state as the length of the nanotube increases. Once again we notice that the CAS-CI energies are significantly relaxed after the NEVPT2 calculations and that there is a strong competition between several singlet states for the ground state at this level. Again, we believe the low-lying spectrum to be correct and some more elaborate calculations (state-specific CASSCF + NEVPT2 or multireference configuration interaction) using larger basis sets should confirm the nature of the CAS-CI ground state.

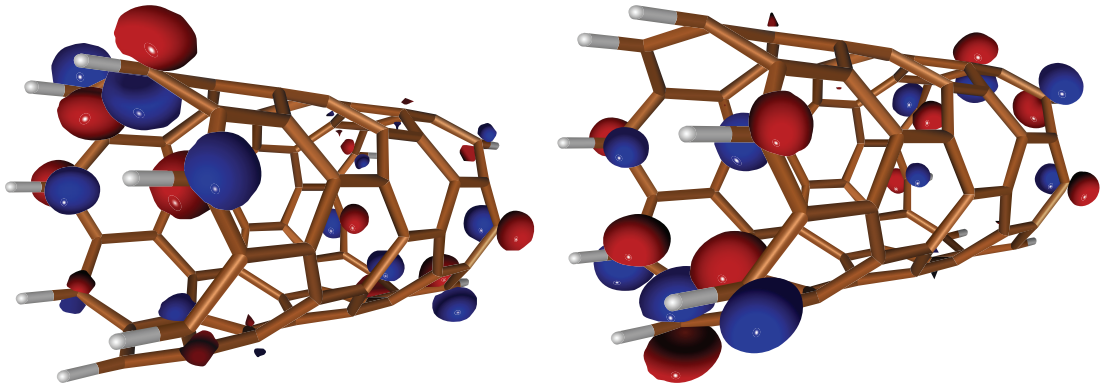

(a) e_{3g}

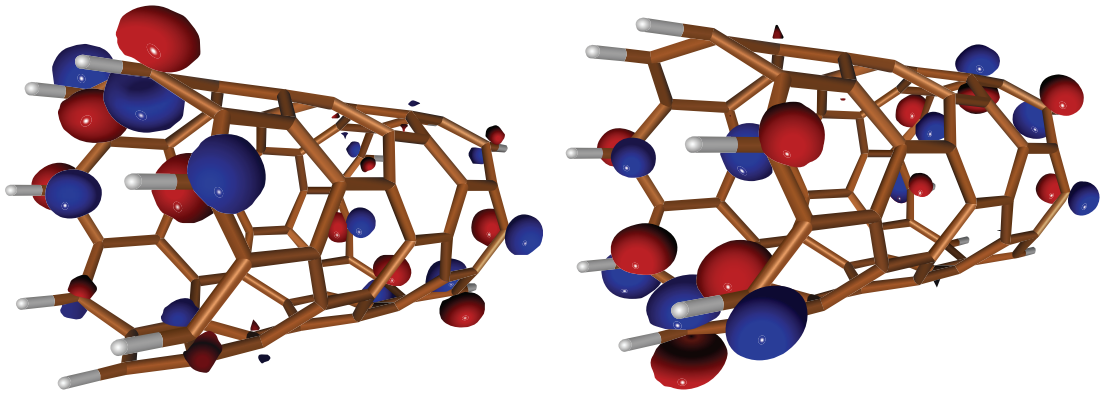

(b) e_{3u}

Figure 8: Active orbitals of nanotube (7_4) as an example of nanotubes with n odd and p even.

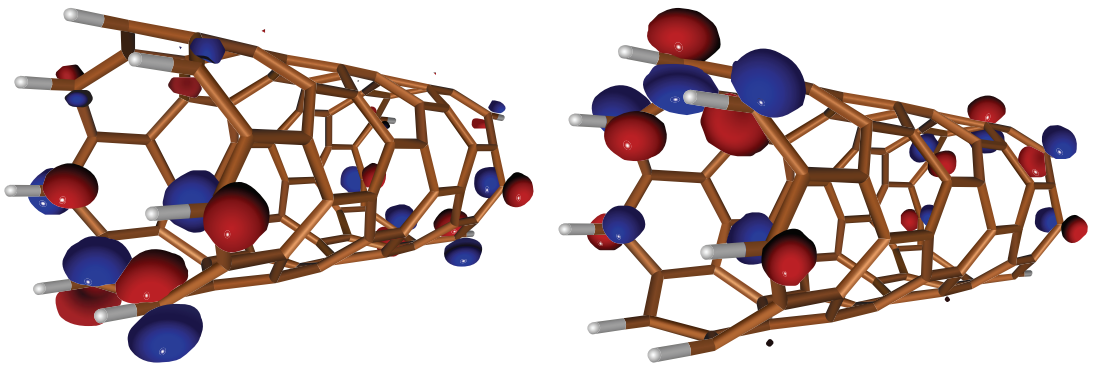

(a) e_3'

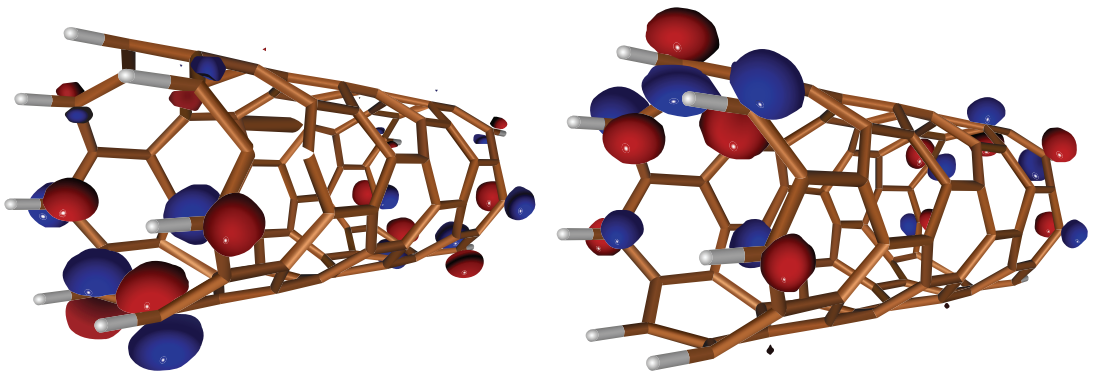

(b) e_3''

Figure 9: Active orbitals for nanotube 7_5 as an example of nanotubes with n odd and p odd.

Table 4: CAS-CI and the NEVPT2 energies in kJ mol^{-1} for the class of nanotubes n_p, with n odd and p even. All possible states for a CAS of four electrons in four orbitals have been calculated.

$n\backslash p$	State	2		4		6	
		CAS-CI	NEVPT2	CAS-CI	NEVPT2	CAS-CI	NEVPT2
7	$^1A_{1g}$	−23.1	−56.5	−0.9	−9.7	$-4 \cdot 10^{-2}$	−2.3
	$^3A_{2u}$	−14.8	−37.8	−0.6	−6.5	$-2 \cdot 10^{-2}$	−1.6
	$^5A_{1g}$	0.0	0.0	0.0	0.0	0.0	0.0
	$^1A_{1u}$	346.4	−49.2	396.9	−4.5	398.7	−1.7
	$^3E_{1u}$	178.0	−17.1	198.5	0.6	199.3	2.7
	$^3E_{1g}$	203.1	−7.7	199.4	1.3	199.4	2.7
	$^1E_{1g}$	406.0	−7.4	398.8	1.7	398.8	2.4
	$^1E_{1u}$	446.6	27.7	569.3	45.9	599.7	97.2
9	$^1A_{1g}$	−13.3	−51.5	−0.5	−15.9	$-2 \cdot 10^{-2}$	−7.5
	$^3A_{2u}$	−8.6	−34.8	−0.3	−10.6	$-1 \cdot 10^{-2}$	−5.0
	$^5A_{1g}$	0.0	0.0	0.0	0.0	0.0	0.00
	$^1A_{1u}$	333.7	−47.4	387.8	−37.9	382.4	−34.2
	$^1E_{1g}$	384.5	−33.5	380.1	−29.3	382.5	−32.4
	$^3E_{1g}$	192.3	−21.9	190.0	−15.3	191.2	−15.5
	$^3E_{1u}$	176.5	−18.0	189.5	−15.5	191.2	−15.5
	$^1E_{1u}$	409.9	52.2	504.0	41.5	547.8	−37.7
11	$^1A_{1g}$	−10.1	−61.6	−0.4	−35.8	$-3 \cdot 10^{-2}$	−27.8
	$^3A_{2u}$	−6.6	−41.6	−0.3	−23.9	$-2 \cdot 10^{-2}$	−18.5
	$^5A_{1g}$	0.0	0.0	0.0	0.0	0.0	0.0
	$^1A_{1u}$	309.1	−52.3	360.8	−88.9	362.9	−87.6
	$^3E_{1g}$	181.4	−38.6	181.1	−39.4	181.5	−43.6
	$^3E_{1u}$	168.6	−26.3	180.7	−39.2	181.4	−43.7
	$^1E_{1u}$	370.5	51.3	449.8	2.8	485.8	−55.9
	$^1E_{1g}$	360.3	51.4	362.3	−70.8	362.9	−82.1

5.2.4. Nanotubes of Type o_o. The orbitals are shown in Figure 9. As in the previous case, there are four valence orbitals located at the edges. The nanotube is characterized by the D_{nh} symmetry, the largest Abelian subgroup being C_{2v}. The two edge orbitals located on one side of σ_v are exactly degenerate with the two located at the opposite side of the σ_v plane; see Table 1. The two pairs of orbitals are quasi-degenerate as a result of the syn- and anti-interaction between the edge orbitals located at the two edges with the anti-interaction being the more stable.

Again, the HF calculations and geometry optimizations were carried out on the quintet state with four orbitals in the open-shell valence space. These calculations were followed by the CAS-CI/NEVPT2 calculations with the same orbitals as active space. The lowest lying singlet and triplet state of each symmetry in the Abelian subgroup were calculated along with the quintet state. The results are presented in Table 5. It is seen that, similar to the previous case, there are two degenerate triplet states and $^1A_1'$ remains the lowest lying state for the nanotubes.

5.2.5. Basis Set Effects. One can see from Tables 6 and 7 that the general trend of the lowest electronic states and the order of magnitude of the CAS-CI energies do not change for the calculations with the cc-pVDZ basis set. This also holds for the lowest states at the NEVPT2 level. An increase of the basis set size involves a relative stabilization of all the levels but the ordering of the levels remains the same.

6. Conclusion

We presented in this paper a *tight binding* and *ab initio* (CAS-CI and NEVPT2) study to evaluate the orbital and vertical electronic state spectrum of short finite zig-zag nanotubes $(n, 0)$. The calculations were carried out on zig-zag nanotubes (n_p) of different size, where n indicates the number of hexagons around the tube, while p is the number of hexagons in the direction of the tube axis. The geometry was relaxed and optimized, by taking into account the full symmetry of the nanotubes. It was found that there are four broad classes of systems, depending on the parity of the parameters n and p. There is a close similarity between the *tight binding* and *ab initio* results with respect to the orbitals pattern close to the Fermi level. This confirms the fact, often seen in several π systems, particularly in the largest ones, that the basic physics of these systems is caught already at this very crude level of approximation. However, a significant *qualitative* difference is found in the case of (e_o) tubes: in this case two *exactly*

Table 5: CAS-CI and the NEVPT2 energies in kJ mol^{-1} for the class of nanotubes n_p, with n odd and p odd. All possible states for a CAS of four electrons in four orbitals have been calculated.

$n\backslash p$	State	1		3		5	
		CAS-CI	NEVPT2	CAS-CI	NEVPT2	CAS-CI	NEVPT2
7	$^1A_1'$	−122.9	−172.2	−4.5	−22.2	−0.2	−4.5
	$^3A_2''$	−70.0	−111.0	−3.0	−14.7	−0.1	−3.0
	$^5A_1'$	0.0	0.0	0.0	0.0	0.0	0.0
	$^3E_1''$	108.7	−65.5	195.2	−2.0	199.2	2.2
	$^3E_1'$	216.4	−37.9	200.0	−2.8	199.4	2.0
	$^1A_1''$	255.1	−10.7	389.4	16.8	398.4	3.6
	$^1E_1'$	422.9	2.0	399.9	−0.1	398.7	2.2
	$^1E_1''$	308.3	40.3	518.4	43.4	590.0	90.3
9	$^1A_1'$	−87.1	−124.5	−2.4	−27.7	−0.1	−10.4
	$^3A_2''$	−50.5	−83.1	−1.6	−18.5	−0.1	−7.0
	$^5A_1'$	0.0	0.0	0.0	0.0	0.0	0.0
	$^3E_1'$	199.4	−45.6	191.1	−19.1	190.3	−15.3
	$^3E_1''$	119.7	−36.0	188.5	−15.8	190.2	−15.0
	$^1E_1'$	369.1	6.3	382.2	−30.2	380.7	−30.6
	$^1A_1''$	260.6	38.7	375.3	3.6	380.5	−28.1
	$^1E_1''$	283.5	92.3	465.9	54.6	526.4	45.0
11	$^1A_1'$	−72.2	−100.6	−2.0	−44.7	−0.1	−30.7
	$^3A_2''$	−42.1	−69.5	−1.3	−29.8	−0.1	−20.4
	$^5A_1'$	0.0	0.0	0.0	0.0	0.0	0.0
	$^3E_1'$	185.5	−55.5	181.0	−39.2	181.3	−41.7
	$^3E_1''$	118.9	−19.5	178.7	−34.5	181.2	−41.3
	$^1E_1'$	329.8	−4.4	361.9	−64.5	362.6	−76.7
	$^1A_1''$	254.0	73.9	355.0	−5.9	362.4	−70.2
	$^1E_1''$	243.6	94.8	409.1	38.4	466.1	−18.1

Table 6: Basis set effects for the nanotubes (6_4) and (6_5).

n_p	State	STO-3G		VDZ	
		CAS-CI	NEVPT2	CAS-CI	NEVPT2
6_4	$^1A_1$	$2 \cdot 10^{-5}$	−2.4	$4 \cdot 10^{-4}$	−3.3
	$^3A_2$	0.0	0.0	0.00	0.00
	$^1E_2$	511.9	165.1	428.1	−11.7
6_5	$^1A_{1g}$	$3 \cdot 10^{-4}$	−3.7	$-1 \cdot 10^{-5}$	−3.8
	$^3A_{2u}$	0.0	0.0	0.0	0.0
	$^1E_{2u}$	535.9	169.3	452.3	−2.0

Table 7: Basis set effects for the nanotubes (7_4) and (7_5).

n_p	State	STO-3G		VDZ	
		CAS-CI	NEVPT2	CAS-CI	NEVPT2
7_4	$^1A_{1g}$	−0.9	−9.7	−0.1	−6.0
	$^3A_{2u}$	−0.6	−6.5	$-4 \cdot 10^{-2}$	−4.0
	$^5A_{1g}$	0.0	0.0	0.0	0.0
	$^1A_{1u}$	396.9	−4.5	299.8	−68.4
	$^3E_{1u}$	198.5	0.6	149.9	−33.4
	$^3E_{1g}$	199.4	1.3	145.0	−33.5
	$^1E_{1g}$	398.8	1.7	299.9	−66.9
	$^1E_{1u}$	569.3	45.9	453.7	−58.6
7_5	$^1A_1'$	−0.2	−4.5	$-1 \cdot 10^{-2}$	−3.1
	$^3A_2''$	−0.1	−3.0	$-7 \cdot 10^{-3}$	−2.0
	$^5A_1'$	0.0	0.0	0.0	0.0
	$^3E_1'$	199.4	2.0	150.1	−32.9
	$^1E_1'$	398.7	2.2	300.2	−66.8
	$^3E_1''$	199.2	2.2	150.1	−32.8
	$^1A_1''$	398.4	3.6	300.2	−66.9
	$^1E_1''$	599.0	90.3	447.1	−45.0

degenerate energy levels are found at the Fermi level in the tight binding description; on the other hand, the energy degeneracy is only approximated at *ab initio* level.

In fact, at *tight binding* level, both (e_e) and (e_o) tubes have two exactly degenerate energy levels at the Fermi level. However, only the degeneracy in the case of (e_e) tubes is a direct consequence of the space point-group symmetry of the tube and is therefore conserved also at *ab initio* level. The (e_o) tubes, on the other hand, have two energy levels that are only approximately degenerate at *ab initio* level, although the split between the levels goes to zero very quickly as a function of the tube length. The nanotubes with an odd parity of n have *four* quasi-degenerate orbitals making up the Fermi level. They are composed of two pairs of strictly degenerate levels: one slightly below and the other one slightly above

the Fermi level. This behavior is qualitatively similar at *tight binding* and *ab initio* level. The vertical energy calculations show that in all the cases the multiplicity of the ground state is a singlet, in systematical accordance with the Ovchinnikov rule [9, 10]. The singlet ground state in all the four cases was found to be of a highly open-shell nature, thus requiring a multireference approach for the calculation of the energy spectrum. As expected, other low-lying states of different spin multiplicities are found at a very small energy above the singlet ground state, indicating the potential interest of these molecular structures in the field of nanotechnology.

In future works we are planning to address the problem of the mobility of the electrons within these structures. To this purpose, it is possible to investigate the response of the system to the action of electric fields along a direction parallel to the tube axis. A further possibility is given by the use of the formalism of the so-called Localization Tensor [48–52], or Second Moment Cumulant of the Position operator, for which an implementation at CAS-SCF level has recently been achieved in our group [53].

Conflict of Interests

The authors declare that there is no conflict of interests regarding the publication of this paper.

Acknowledgments

This work was partly supported by the French "Centre National de la Recherche Scientifique" (CNRS, also under the PICS action 4263) and ANR under the ANR/DFG Joint Project MITLOW (ANR-11-INTB-1009), the HPC resources of CALMIP under the allocation 2011-[p1048], and the Italian Ministry of University and Research (MUR). The authors would also like to thank the Erasmus Mundus Program, funded by the European Commission, and in particular its project "TCCM Euromaster on Theoretical Chemistry and Computational Modelling," for partial support of this work through a generous grant to one of the present authors (Vijay Gopal Chilkuri).

References

[1] K. S. Novoselov, A. K. Geim, S. V. Morozov et al., "Electric field effect in atomically thin carbon films," *Science*, vol. 306, no. 5696, pp. 666–669, 2004.

[2] K. S. Novoselov, A. K. Geim, S. V. Morozov et al., "Two-dimensional gas of massless Dirac fermions in graphene," *Nature*, vol. 438, no. 7065, pp. 197–200, 2005.

[3] W. Andreoni, *The Physics of Fullerene-Based and Fullerene-Related Materials*, Springer, Berlin, Germany, 2000.

[4] C. Lee, X. Wei, J. W. Kysar, and J. Hone, "Measurement of the elastic properties and intrinsic strength of monolayer graphene," *Science*, vol. 321, no. 5887, pp. 385–388, 2008.

[5] J. Chen, S. Chen, X. Zhao, L. V. Kuznetsova, S. S. Wong, and I. Ojima, "Functionalized single-walled carbon nanotubes as rationally designed vehicles for tumor-targeted drug delivery," *Journal of the American Chemical Society*, vol. 130, no. 49, pp. 16778–16785, 2008.

[6] J.-C. Charlier, X. Blase, and S. Roche, "Electronic and transport properties of nanotubes," *Reviews of Modern Physics*, vol. 79, no. 2, pp. 677–732, 2007.

[7] B. Trauzettel, D. V. Bulaev, D. Loss, and G. Burkard, "Spin qubits in graphene quantum dots," *Nature Physics*, vol. 3, no. 3, pp. 192–196, 2007.

[8] A. H. Castro Neto, F. Guinea, N. M. R. Peres, K. S. Novoselov, and A. K. Geim, "The electronic properties of graphene," *Reviews of Modern Physics*, vol. 81, no. 1, pp. 109–162, 2009.

[9] I. A. Misurkin and A. A. Ovchinnikov, "The electronic structures and properties of polymeric molecules with conjugated bonds," *Russian Chemical Reviews*, vol. 46, no. 10, pp. 967–987, 1977.

[10] A. A. Ovchinnikov, "Multiplicity of the ground state of large alternant organic molecules with conjugated bonds," *Theoretica Chimica Acta*, vol. 47, no. 4, pp. 297–304, 1978.

[11] E. H. Lieb, "Two theorems on the Hubbard model," *Physical Review Letters*, vol. 62, no. 10, pp. 1201–1204, 1989.

[12] J. F. Rossier and J. J. Palacios, "Magnetism in graphene nanoislands," *Physical Review Letters*, vol. 99, Article ID 177204, 2007.

[13] M. El Khatib, S. Evangelisti, T. Leininger, and G. L. Bendazzoli, "A theoretical study of closed polyacene structures," *Physical Chemistry Chemical Physics*, vol. 14, no. 45, pp. 15666–15676, 2012.

[14] A. Rochefort, D. R. Salahub, and P. Avouris, "Effects of finite length on the electronic structure of carbon nanotubes," *Journal of Physical Chemistry B*, vol. 103, no. 4, pp. 641–646, 1999.

[15] O. Hod and G. E. Scuseria, "Half-metallic zigzag carbon nanotube dots," *ACS Nano*, vol. 2, no. 11, pp. 2243–2249, 2008.

[16] C. M. Ruiz and S. D. Dalosto, "Electronic and magnetic changes in a finite-sized single-walled zigzag carbon nanotube embedded in water," *The Journal of Physical Chemistry C*, vol. 117, no. 1, pp. 633–638, 2013.

[17] S. Tang and Z. Cao, "Electronic and magnetic properties of nitrogen-doped finite-size and open-ended zigzag carbon nanotubes," *Computational Materials Science*, vol. 50, no. 6, pp. 1917–1924, 2011.

[18] J. Wu and F. Hagelberg, "Magnetism in finite-sized single-walled carbon nanotubes of the zigzag type," *Physical Review B*, vol. 79, Article ID 115436, 2009.

[19] M. Margańska, M. del Valle, S. H. Jhang, C. Strunk, and M. Grifoni, "Localization induced by magnetic fields in carbon nanotubes," *Physical Review B—Condensed Matter and Materials Physics*, vol. 83, no. 19, Article ID 193407, 2011.

[20] W. Chun-Shian and C. Jeng-Da, "Electronic properties of zigzag graphene nanoribbons studied by TAO-DFT," *Journal of Chemical Theory and Computation*, vol. 11, no. 5, pp. 2003–2011, 2015.

[21] R. Sundaram, S. Scheiner, A. K. Roy, and T. Kar, "B=N bond cleavage and BN ring expansion at the surface of boron nitride nanotubes by iminoborane," *Journal of Physical Chemistry C*, vol. 119, no. 6, pp. 3253–3259, 2015.

[22] Y. Wang, G. Fang, J. Ma, and Y. Jiang, "Facial dissociations of water molecules on the outside and inside of armchair single-walled silicon nanotubes: theoretical predictions from multilayer quantum chemical calculations," *Theoretical Chemistry Accounts*, vol. 130, no. 2, pp. 463–473, 2015.

[23] W. Mizukami, Y. Kurashige, and T. Yanai, "More π electrons make a difference: emergence of many radicals on graphene nanoribbons studied by Ab initio DMRG theory," *Journal of Chemical Theory and Computation*, vol. 9, no. 1, pp. 401–407, 2013.

[24] A. Donarini, A. Yar, and M. Grifoni, "Spectrum and Franck-Condon factors of interacting suspended single-wall carbon nanotubes," *New Journal of Physics*, vol. 14, no. 2, pp. 23045–23067, 2012.

[25] A. Dirnaichner, M. Grifoni, A. Pruing, D. Steininger, A. K. Hüttel, and C. Strunk, "Transport across a carbon nanotube quantum dot contacted with ferromagnetic leads: experiment and non-perturbative modeling," *Physical Review B*, vol. 91, no. 19, Article ID 195402, 2015.

[26] P. R. Wallace, "The band theory of graphite," *Physical Review*, vol. 71, pp. 622–634, 1947.

[27] M. El Khatib, S. Evangelisti, T. Leininger, and G. L. Bendazzoli, "Partly saturated polyacene structures: a theoretical study," *Journal of Molecular Modeling*, vol. 20, no. 7, article 2284, 2014.

[28] R. Hoffmann, "An extended Hückel theory. I. Hydrocarbons," *The Journal of Chemical Physics*, vol. 39, no. 6, article 1397, 1963.

[29] T. Helgaker, P. Jørgensen, and J. Olsen, *Molecular Electronic-Structure Theory*, John Wiley & Sons, New York, NY, USA, 2000.

[30] B. O. Roos, "The complete active space self-consistent field method and its applications in electronic structure calculations," in *Advances in Chemical Physics: Ab Initio Methods in Quantum Chemistry*, K. P. Lawle, Ed., vol. 69, part 2, pp. 399–445, John Wiley & Sons, New York, NY, USA, 2007.

[31] B. O. Roos and K. Andersson, "Multiconfigurational perturbation theory with level shift—the Cr_2 potential revisited," *Chemical Physics Letters*, vol. 245, no. 3, pp. 215–223, 1995.

[32] G. Ghigo, B. O. Roos, and P. A. Malmqvist, "A modified definition of the zeroth-order Hamiltonian in multiconfigurational perturbation theory (CASPT2)," *Chemical Physics Letters*, vol. 396, no. 1–3, pp. 142–149, 2004.

[33] S. Evangelisti, G. L. Bendazzoli, and A. Monari, "Charge state of metal atoms on oxide supports: a systematic study based on simulated infrared spectroscopy and density functional theory," *Theoretical Chemistry Accounts*, vol. 126, no. 3, pp. 265–273, 2010.

[34] G. L. Bendazzoli, S. Evangelisti, A. Monari, and R. Resta, "Kohn's localization in the insulating state: one-dimensional lattices, crystalline versus disordered," *The Journal of Chemical Physics*, vol. 133, no. 6, Article ID 064703, 2010.

[35] A. Monari and S. Evangelisti, "Finite-size effects in graphene nanostructures," in *Physics and Applications of Graphene: Theory*, S. Mikhailov, Ed., chapter 14, p. 303, InTech, Rijeka, Croatia, 2011.

[36] W. J. Hehre, R. F. Stewart, and J. A. Pople, "Self-consistent molecular-orbital methods. I. Use of gaussian expansions of slater-type atomic orbitals," *The Journal of Chemical Physics*, vol. 51, no. 6, pp. 2657–2664, 1969.

[37] T. H. Dunning Jr., "Gaussian basis sets for use in correlated molecular calculations. I. The atoms boron through neon and hydrogen," *The Journal of Chemical Physics*, vol. 90, article 1007, 1989.

[38] P. Knowles and H. J. Werner, "Molpro quantum chemistry package," http://www.molpro.net.

[39] B. Roos, P. R. Taylor, and P. E. M. Siegbahn, "A complete active space SCF method (CASSCF) using a density matrix formulated super-CI approach," *Chemical Physics*, vol. 48, no. 2, pp. 157–173, 1980.

[40] C. Angeli, R. Cimiraglia, S. Evangelisti, T. Leininger, and J.-P. Malrieu, "Introduction of n-electron valence states for multireference perturbation theory," *Journal of Chemical Physics*, vol. 114, no. 23, Article ID 10252, 2001.

[41] C. Angeli, R. Cimiraglia, and J.-P. Malrieu, "*n*-electron valence state perturbation theory: a spinless formulation and an efficient implementation of the strongly contracted and of the partially contracted variants," *Journal of Chemical Physics*, vol. 117, no. 20, pp. 9138–9153, 2002.

[42] C. Angeli, M. Pastore, and R. Cimiraglia, "New perspectives in multireference perturbation theory: the *n*-electron valence state approach," *Theoretical Chemistry Accounts*, vol. 117, no. 5-6, pp. 743–754, 2007.

[43] H.-J. Werner and P. J. Knowles, "A second order multiconfiguration SCF procedure with optimum convergence," *The Journal of Chemical Physics*, vol. 82, no. 11, pp. 5053–5063, 1985.

[44] P. J. Knowles and H.-J. Werner, "An efficient second-order MC SCF method for long configuration expansions," *Chemical Physics Letters*, vol. 115, no. 3, pp. 259–267, 1985.

[45] D. Yu, E. M. Lupton, H. J. Gao, C. Zhang, and F. Liu, "A unified geometric rule for designing nanomagnetism in graphene," *Nano Research*, vol. 1, no. 6, pp. 497–501, 2008.

[46] C. Angeli, "On the nature of the $\pi \rightarrow \pi^*$ ionic excited states: the V state of ethene as a prototype," *Journal of Computational Chemistry*, vol. 30, no. 8, pp. 1319–1333, 2009.

[47] C. Angeli and C. J. Calzado, "The role of the magnetic orbitals in the calculation of the magnetic coupling constants from multireference perturbation theory methods," *The Journal of Chemical Physics*, vol. 137, no. 3, Article ID 034104, 2012.

[48] R. Resta and S. Sorella, "Electron localization in the insulating state," *Physical Review Letters*, vol. 82, no. 2, pp. 370–373, 1999.

[49] C. Sgiarovello, M. Peressi, and R. Resta, "Electron localization in the insulating state: application to crystalline semiconductors," *Physical Review B*, vol. 64, no. 11, Article ID 115202, 2001.

[50] R. Resta, "Why are insulators insulating and metals conducting?" *Journal of Physics Condensed Matter*, vol. 14, no. 20, pp. R625–R656, 2002.

[51] R. Resta, "Electron localization in the quantum hall regime," *Physical Review Letters*, vol. 95, Article ID 196805, 2005.

[52] R. Resta, "The insulating state of matter: a geometrical theory," *The European Physical Journal B*, vol. 79, no. 2, pp. 121–137, 2011.

[53] M. El Khatib, T. Leininger, G. L. Bendazzoli, and S. Evangelisti, "Computing the Position-Spread tensor in the CAS-SCF formalism," *Chemical Physics Letters*, vol. 591, pp. 58–63, 2014.